 CMES, vol.61, no.2, pp.133-154, 2010

Elastic Moduli of Woven Fabric Composite by Meshless Local Petrov-Galerkin (MLPG) Method

P.H. Wen[1] and M.H. Aliabadi[2]

Abstract: A meshless local Petrov-Galerkin method, for the micro-mechanical material model of woven fabric composite material is presented in this paper. The material models are based on a repeated unit cell approach and two smooth fibre modes. A unit step function is used as the test functions in the local weak-form which leads to local boundary integral equations. The analysed domain is divided into small sub-domains and the radial basis function interpolation without element mesh is adopted. The woven fabric composite elastic moduli evaluated have been shown to be in good agreement with finite element results.

Keywords: meshless local Petrov-Galerkin method, woven fabric composites, elastic moduli

1 Introduction

Recent advances in Meshless method have demonstrated its advantage over the finite element method in several applications [Atluri, S.N.; Zhu, T.; (1998a; 1998b; 1990), Atluti(2004), Atluri, Liu, Han(2005); Sladek, Sladek, Krivacek and Zhang (2005); Sladek, Sladek, Tanaka and Zhang (2005); Wen, P.H., Aliabadi, M.H.; Liu, Y.W.(2008), Wen and Aliabadi(2010)]. A key feature of these methods is that they do not require a structured grid and therefore are better suited to modelling complex geometries or moving boundary problems. Atluri and co-workers presented a family of the meshless local Petrov-Galerkin (MLPG) method, based on the Local weak Petrov-Galerkin formulation for arbitrary partial differential equations [see Atluri et al (1998a and 199b)] with moving least-square (MLS) approximation]. MLPG is reported to provide a rational basis for constructing meshless methods with a greater degree of flexibility. The Finite Difference Method (FDM), within the framework of the Meshless Local Petrov-Galerkin approach, is proposed for

[1] School of Engineering and Material Sciences, Queen Mary, University of London, London, UK, E1 4NS
[2] Department of Aeronautics, Imperial College, London, UK, SW7 2BY

solving solid mechanics problems [Atluri and Zhu (1999)]. The implementation of a three-dimensional dynamic code, for contact, impact, and penetration mechanics, based on the Meshless Local Petrov-Galerkin approach has been presented [Atluri, Liu; Han(2005)]. A meshless computational method based on the local Petrov-Galerkin approach for the analysis of shell structures is presented for three dimensional solid, allowing the use of completely 3-D constitutive models [Han, Liu, Ranjendran, Atluri(2006)]. A meshless method based on the local Petrov-Galerkin approach is proposed for the solution of boundary value problems for coupled thermo-electro-mechanical fields and crack analysis in two-dimensional (2-D) and three-dimensional (3-D) axisymmetric piezoelectric solids with continuously varying material properties [Jarak, Soric,Hoster92007); Sladek, Saldek, Zhang, Solek (2007a)].

The Local Boundary Integral Equation method (LBIE) with moving least square and polynomial radial basis function (RBF) has been developed by Sladek, Saldek, Zhang, Solek , Starek(2007b) and Sladek, Sladek and Zhang (2004) for boundary value problems in anisotropic non-homogeneous media including functionally graded materials. Both methods (MLPG and LBIE) are meshless, as no domain/boundary meshes are required in these two approaches. Application of the MPLG to elastodynamic and shear deformable shells can be found in [Wen and Aliabadi(2008a, 2008b, 2009) and Sladek, Sladek, Wen, Aliabadi(2006), respectively. A comprehensive review of meshless methods can be found in the book by Atluri (2004).

Woven composite materials are increasingly utilized as primary structural components due to their low weight to strength ratio. In traditional fibre reinforced composites the fibres are aligned parallel to the plane direction providing an excellent in-plane mechanical property, but are poor in the transverse plane mechanical properties. Woven composites on the other hand are developed to provide increase mechanical properties in both the in-plane and transverse directions. The development of the woven composite technology relies heavily on a better understanding of its micromechanical behaviour. To circumvent large computational models when analyzing these complex composite structures many approaches have been developed towards homogenization of macroscopic properties. An early model for the analysis of woven fabric composites can be found in the work by Ishikawa (1981) and Ishikawa and Chou(1983). The finite element analysis and approximated analytical analysis were carried out by Chung and Tamma (1999) and Tanov and Tabiei (2001). Wen and Aliabadi (2009b) developed an element-free Galerkin method to composite material for the evaluation of functional elastic moduli in the computational volume cell. Other applications of meshless method to composite materials can be found in [Dang,Thi, D and Sanker (2007, 2008)].

In this paper, the meshless local Petrov-Galerkin method is developed for the woven fabric composites. The meshless method for the problems of micro-mechanical models is used for the evaluation of functional elastic moduli in the computational volume cell. The accuracy of MLPG method is compared with the results given by FEM [Hardy (1971) and Marrey and Sanker (1977)] and the element-free Galerkin method [Wen and Aliabadi (2009)].

2 The meshless local Petrov-Galerkin method

Consider a linear elastic body in a three dimensional domain Ω with boundary $\partial\Omega$. For woven fabric composites, Hooke's law can also be written, in matrix form, as

$$\sigma = \begin{Bmatrix} \sigma_{11} \\ \sigma_{22} \\ \sigma_{33} \\ \sigma_{12} \\ \sigma_{23} \\ \sigma_{31} \end{Bmatrix} = \begin{bmatrix} C_{11} & C_{12} & C_{13} & C_{14} & C_{15} & C_{16} \\ C_{21} & C_{22} & C_{23} & C_{24} & C_{25} & C_{26} \\ C_{31} & C_{32} & C_{33} & C_{34} & C_{35} & C_{36} \\ C_{41} & C_{42} & C_{43} & C_{44} & C_{45} & C_{46} \\ C_{51} & C_{52} & C_{53} & C_{54} & C_{55} & C_{56} \\ C_{61} & C_{62} & C_{63} & C_{64} & C_{65} & C_{66} \end{bmatrix} \begin{Bmatrix} \varepsilon_{11} \\ \varepsilon_{22} \\ \varepsilon_{33} \\ \varepsilon_{12} \\ \varepsilon_{23} \\ \varepsilon_{31} \end{Bmatrix} = \mathbf{C}(x,y)\boldsymbol{\varepsilon} \tag{1}$$

where $C_{ij} = C_{ji}$ denotes the elasticity tensor, σ_{ij} and ε_{ij} are stress and strain tensors. The equations of equilibrium can be written as

$$\sigma_{ij,j} + f_i = 0, \tag{2}$$

where f_i is the body force. The boundary conditions are given as

$$u_i = \bar{u}_i \text{ on } \Gamma_u$$
$$t_i = \sigma_{ij} n_j = \bar{t}_i \text{ on } \Gamma_t$$

in which $\bar{u}_i$ and $\bar{t}_i$ are the prescribed displacements and tractions respectively on the displacement boundary Γ_u and on the traction boundary Γ_t, and n_i is the unit normal outward to the boundary Γ. In the local Petrov-Galerkin approaches, the weak form of differential equation over a local sub-domain Ω_s can be written as

$$\int_{\Omega_s} (\sigma_{ij,j} + f_i) u_i^* d\Omega = 0 \tag{3}$$

where u_i^* is a test function. By use of divergence theorem, equation (3) can be rewritten in a symmetric weak form as

$$\int_{\partial\Omega_s} \sigma_{ij} n_j u_i^* d\Gamma - \int_{\Omega_s} (\sigma_{ij} u_{i,j}^* - f_i u_i^*) d\Omega = 0 \tag{4}$$

If there is an intersection between the local boundary and the global boundary, a local symmetric weak form in linear elasticity may be written as

$$\int_{\Omega_s} \sigma_{ij} u^*_{i,j} d\Omega - \int_{L_a} t_i u^*_i d\Gamma - \int_{\Gamma_{su}} t_i u^*_i d\Gamma = \int_{\Gamma_{st}} \bar{t}_i u^*_i d\Gamma + \int_{\Omega_s} f_i u^*_i d\Omega \tag{5}$$

in which, $\partial\Omega_s = \Gamma_s \cup L_s$, Γ_s is a part of the local boundary located on the global boundary and L_s is the other part of the local boundary inside the sub-domain Ω_s; $\Gamma_{su} = \Gamma_s \cap \Gamma_u$ is the intersection between the local boundary $\partial\Omega_s$ and the global displacement boundary Γ_u; $\Gamma_{st} = \Gamma_s \cap \Gamma_t$ is a part of the traction boundary as shown in Figure 1.

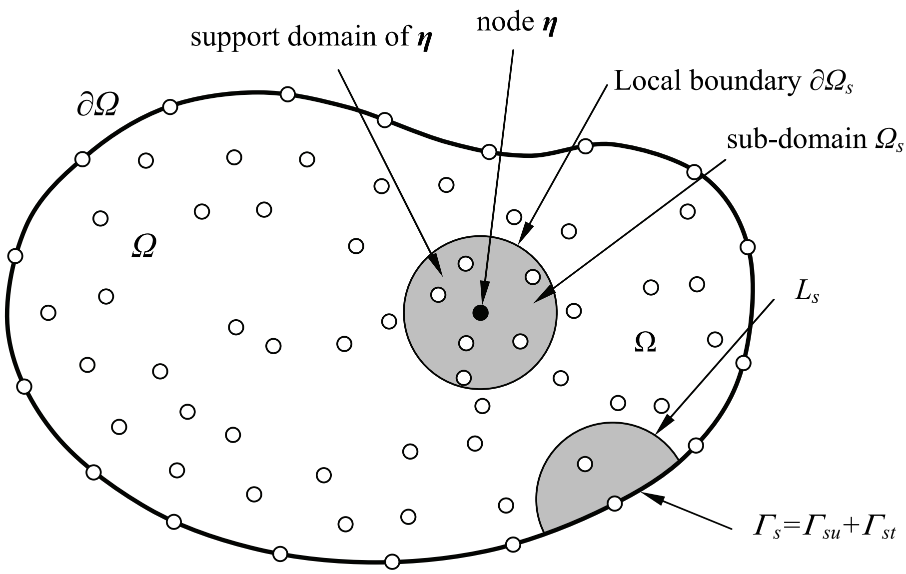

Figure 1: Local boundaries for weak formulation, the domain $\Omega_{s}{}_s$ for RBF approximation of the trial function, and support area of weight function around node ξ.

The local weak forms (4) and (5) are a starting point to derive local boundary integral equations if appropriate test functions are selected. A unit step functions can be used as the test functions u^*_i in each sub-domain

$$u^*_i(\mathbf{x}) = \begin{cases} 1 & \text{at } \mathrm{x} \in (\Omega_\mathrm{s} \cup \partial\Omega_s) \\ 0 & \text{at } \mathrm{x} \notin \Omega_\mathrm{s} \end{cases} . \tag{6}$$

Then, the local weak forms (4) and (5) are transformed into simple local boundary integral equations (equilibrium of sub-domain) as

$$\int_{\partial\Omega_s} t_i d\Gamma = -\int_{\Omega_s} f_i d\Omega \tag{7}$$

and

$$\int_{L_a+\Gamma_{su}} t_i d\Gamma = -\int_{\Gamma_{st}} \bar{t}_i d\Gamma - \int_{\Omega_s} f_i d\Omega \tag{8}$$

By the use of shape function, we then have$\mathbf{u} = \mathbf{\Phi}\hat{\mathbf{u}}$, $\boldsymbol{\varepsilon} = \mathbf{B}\hat{\mathbf{u}}$, where $\mathbf{\Phi} = \{\varphi_1, \varphi_2, ..., \varphi_n\}$ is shape function discussed in section 3. Matrix $\mathbf{B}$ is defined by

$$\mathbf{B}_i = \begin{bmatrix} \frac{\partial\varphi_i}{\partial x} & 0 & 0 \\ 0 & \frac{\partial\varphi_i}{\partial y} & 0 \\ 0 & 0 & \frac{\partial\varphi_i}{\partial z} \\ \frac{\partial\varphi_i}{\partial y} & \frac{\partial\varphi_i}{\partial y} & 0 \\ 0 & \frac{\partial\varphi_i}{\partial z} & \frac{\partial\varphi_i}{\partial y} \\ \frac{\partial\varphi_i}{\partial z} & 0 & \frac{\partial\varphi_i}{\partial x} \end{bmatrix}, \tag{9}$$

$\hat{u}_i(\boldsymbol{\xi})$ denotes the nodal value at point $\boldsymbol{\xi}_k = \{x_k, y_k, z_k\}$, $k = 1, 2, ..., n$, and n is the total number of nodes in the sub-domain as shown in Figure 1. Therefore the stress tensor can be written as

$$\sigma = \mathbf{C}(\mathbf{x})\mathbf{B}\hat{\mathbf{u}} \tag{10}$$

and traction tensor on the boundary $\partial\Omega_s$ is

$$\mathbf{t} = \mathbf{n}\cdot\sigma = \mathbf{N}(\mathbf{x})\mathbf{C}(\mathbf{x})\mathbf{B}\hat{\mathbf{u}} \tag{11}$$

where the matrix $\mathbf{N}(\mathbf{x})$ is related to the normal vector $\mathbf{n}$ of $\partial\Omega_s$.

3 Shape function and approximation schemes

Consider a sub-domain $\partial\Omega_s$shown in Figure 1, which is the neighbourhood of a point $\boldsymbol{\eta}$ $(= \{x, y, z\})$ and is considered as the domain of definition of the RBF approximation for the trail function at $\boldsymbol{\eta}$ and also called as support domain to an arbitrary point $\boldsymbol{\eta}$. To interpolate the distribution of function u in the sub-domain

$\partial\Omega_s$over a number of randomly distributed nodes $\boldsymbol{\xi}\,[=\{\boldsymbol{\xi}_1,\xi_2,...,\boldsymbol{\xi}_n\}\,,\ \boldsymbol{\xi}_i=(x_i,y_i,z_i)$, i=1,2,. . . ,n], the approximation of function u at the point $\boldsymbol{\eta}$ can be expressed by

$$u(\boldsymbol{\eta})=\sum_{k=1}^{n}R_k(\boldsymbol{\eta},\xi)a_k=\mathbf{R}^T(\boldsymbol{\eta},\boldsymbol{\xi})\mathbf{a}(\boldsymbol{\eta}) \tag{12}$$

where $\mathbf{R}^T(\boldsymbol{\eta},\boldsymbol{\xi})=\{R_1(\boldsymbol{\eta},\boldsymbol{\xi}),R_2(\boldsymbol{\eta},\boldsymbol{\xi}),...,R_n(\boldsymbol{\eta},\boldsymbol{\xi})\}$ is the set of radial basis functions centred around the point $\boldsymbol{\eta}$, $\{a_k\}_{k=1}^n$ are the unknown coefficients to be determined. The radial basis function selected multi-quadrics [Hardy (1971), Marrey and Sanker(1977)] as

$$R_k(\boldsymbol{\eta},\boldsymbol{\xi})=\sqrt{c^2+\alpha_1(x-x_k)^2+\alpha_2(y-y_k)^2+\alpha_3(z-z_k)^2} \tag{13}$$

where c is a free parameter (is chosen to unit in this paper) and α_i are scale factors. From the interpolation equation (12) for the compact support RBFs a linear system for the unknowns coefficients $\mathbf{a}$ is obtained as

$$\mathbf{R}_0\mathbf{a}=\mathbf{u} \tag{14}$$

where

$$\mathbf{u}^T=\{u_1,u_2,...,u_n\} \tag{15}$$

are the nodal values, $u_i=u(\boldsymbol{\xi}_i)$ and

$$\mathbf{R}_0(\boldsymbol{\xi})=\begin{bmatrix} R_1(\boldsymbol{\xi}_1) & R_2(\boldsymbol{\xi}_1) & ... & R_n(\boldsymbol{\xi}_1)\\ R_1(\boldsymbol{\xi}_2) & R_2(\boldsymbol{\xi}_2) & ... & R_n(\boldsymbol{\xi}_2)\\ . & . & \cdots & .\\ . & . & \cdots & .\\ . & . & \cdots & .\\ R_1(\boldsymbol{\xi}_n) & R_2(\boldsymbol{\xi}_n) & ... & R_n(\boldsymbol{\xi}_n)\end{bmatrix}. \tag{16}$$

It is evident that the interpolation of field variable is satisfied exactly at each node. As the RBFs are positive definite, the matrix $\mathbf{R}_0$ is assured to be invertible. Therefore, we can obtain the vector of unknowns from Eq. (14)

$$\mathbf{a}=\mathbf{R}_0^{-1}(\boldsymbol{\xi})\mathbf{u}(\boldsymbol{\xi}). \tag{17}$$

So that the approximation $u(\mathbf{y})$ can be represented, at domain point $\mathbf{y}$, as

$$u(\boldsymbol{\eta})=\mathbf{R}^T(\boldsymbol{\eta})\mathbf{R}_0^{-1}(\boldsymbol{\xi})\mathbf{u}(\boldsymbol{\xi})=\boldsymbol{\Phi}(\boldsymbol{\eta},\boldsymbol{\xi})\mathbf{u}(\boldsymbol{\xi})=\sum_{k=1}^{n}\phi_k u_k \tag{18}$$

were the nodal shape function are defined by

$$\mathbf{\Phi}(\boldsymbol{\eta},\boldsymbol{\xi}) = \mathbf{R}^T(\boldsymbol{\eta})\mathbf{R}_0^{-1}(\boldsymbol{\xi}). \tag{19}$$

It is worth noting that the shape function depends uniquely on the distribution of scattered nodes within the support domain and has the Kronecker Delta property. As the inverse matrix of coefficient $\mathbf{R}_0^{-1}(\boldsymbol{\xi})$ is function only of distributed node $\mathbf{x}$ in the support domain, it is much simpler to evaluate the partial derivatives of shape function. In order to guarantee unique solution of the interpolation problem, a polynomial term is added to the interpolation (18), giving

$$u(\boldsymbol{\eta}) = \sum_{k=1}^{n} R_k(\boldsymbol{\eta},\xi)a_k + \sum_{j=1}^{t} P_j(\boldsymbol{\eta})b_j = \mathbf{R}_0(\boldsymbol{\eta},\boldsymbol{\xi})\mathbf{a} + \mathbf{P}(\boldsymbol{\eta})\mathbf{b} \tag{20}$$

along with the constraints

$$\sum_{j=1}^{t} P_k(\boldsymbol{\xi}_j)a_j = 0, \quad 1 \le k \le t \tag{21}$$

where $\{P_k\}_{k=1}^{t}$ is a basis for P_{m-1}, the set of d-variate polynomials of degree $\le m-1$, and

$$t = \left(\begin{bmatrix} m+d-1 \\ d \end{bmatrix} \right) \tag{22}$$

is the dimension of P_{m-1}. A set of linear equations can be written, in the matrix form, as

$$\mathbf{R}_0\mathbf{a} + \mathbf{P}^T\mathbf{b} = \mathbf{u}, \quad \mathbf{Pa} = \mathbf{0} \tag{23}$$

where matrix

$$P(\boldsymbol{\xi}) = \begin{bmatrix} P_1(\boldsymbol{\xi}_1) & P_2(\boldsymbol{\xi}_1) & \dots & P_t(\boldsymbol{\xi}_1) \\ P_1(\boldsymbol{\xi}_2) & P_2(\boldsymbol{\xi}_2) & \dots & P_t(\boldsymbol{\xi}_2) \\ . & . & \dots & . \\ . & . & \dots & . \\ . & . & \dots & . \\ P_1(\boldsymbol{\xi}_n) & P_2(\boldsymbol{\xi}_n) & \dots & P_t(\boldsymbol{\xi}_n) \end{bmatrix}. \tag{24}$$

Solving these equations in Eq.(23) gives

$$\mathbf{b} = \left(\mathbf{P}^T\mathbf{R}_0^{-1}\mathbf{P}\right)^{-1}\mathbf{P}^T\mathbf{R}_0^{-1}\mathbf{u}, \quad \mathbf{a} = \mathbf{R}_0^{-1}\left[\mathbf{I} - \mathbf{P}\left(\mathbf{P}^T\mathbf{R}_0^{-1}\mathbf{P}\right)^{-1}\mathbf{P}^T\mathbf{R}_0^{-1}\right]\mathbf{u} \tag{25}$$

where **I** denotes the diagonal unit matrix. Substituting the coefficients **a** and **b** from Eq. (25) into Eq. (20), we can obtain the approximation of the field function in terms of the nodal values

$$u(\boldsymbol{\eta}) = \sum_{k=1}^{n} \phi_k(\boldsymbol{\eta},\boldsymbol{\xi})u(\boldsymbol{\xi}_k). \tag{26}$$

It is clear that the coefficient **a** and **b** are functions of nodal positions **x** with nodal values **u**. Furthermore, by substituting the RBF approximations (7) and (8) for the unknown fields into the local boundary domain integral equation (7), we obtain the discretized equations (LIE)

$$\int_{\partial\Omega_s} \sum_{k=1}^{n} \mathbf{N}(\mathbf{x})\mathbf{C}(\mathbf{x})\mathbf{B}^k(\mathbf{x})\hat{\mathbf{u}}^k d\Gamma = -\int_{\Omega_s} \mathbf{F}(\mathbf{x})d\Omega \tag{27}$$

and

$$\int_{L_s+\Gamma_{su}} \sum_{k=1}^{n} \mathbf{N}(\mathbf{x})\mathbf{C}(\mathbf{x})\mathbf{B}^k(\mathbf{x})\hat{\mathbf{u}}^k d\Gamma = -\int_{\Gamma_{st}} \bar{\mathbf{t}}(\mathbf{x})d\Gamma - \int_{\Omega_s} \mathbf{F}(\mathbf{x})d\Omega \tag{28}$$

from equation (8). It is worth to point out that the essential boundary conditions can be imposed directly with the use of the RBF approximation. Although the essential boundary conditions are satisfied on the prescribed displacement boundary, these conditions are still not satisfied for all points on the boundary Γ_{su} except the nodal points.

It is useful to point out for multiscale problem that the integral equation (7) can be written as

$$\int_{\partial\Omega_s^I+\partial\Omega_s^{II}} t_i d\Gamma = -\int_{\Omega_s^I+\Omega_s^{II}} f_i d\Omega \tag{29}$$

The local integral boundary with interface is shown in Figure 2. It is apparent that the continuity of the displacement is satisfied everywhere in the local domain including the interface. But there are jumps for tractions on the interface in each local integral domain. However, if the size of the local domain is small enough, the influence of these discontinuities of the tractions can be ignored. Therefore, in the numerical implementation, the interface does not appear in the local integral equation (29). In the numerical procedure, we do not need to distribute node on the interface and consider the continuity of tractions. This simplification works very well for multiscale problems. But the interface (surface) is used in the numerical procedure to define the boundaries for each different material.

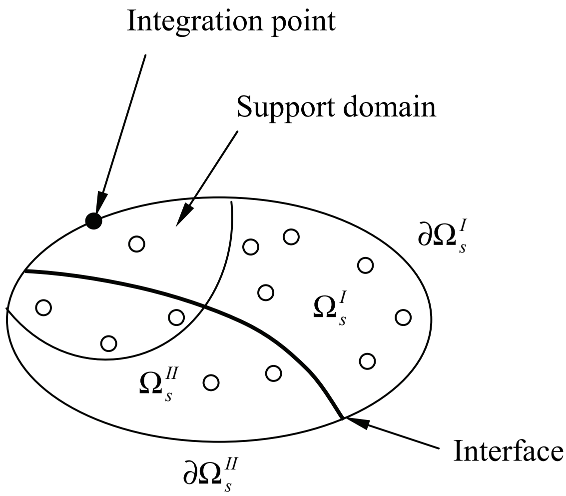

Figure 2: Interfacial problem.

4 The volume cell models

The micromechanical model is based on the method of cells, which consists in dividing the representative volume cell (RVC) in different blocks or cells, each of which can be further divided into sub-cells. These sub-cells are an idealization of actual RVC's sub-volumes, i.e. part of a unidirectional (UD) yarn or a pure matrix region as shown in Figure 3. The entire woven fabric lamina can be constructed by using the RVC shown in Figure 3(b) as a building block. Assuming that the fiber yarns in both direction (the fill and warp) have the same structure and properties, that part of the woven RVC can be constructed using four-cell model as shown in Figure 3(c). Therefore, only a quarter of the composite's RVE needs to be considered to derive the homogenized stiffness properties of the whole woven composite's RVC. The homogenized stiffness properties of the woven composite's RVC are then used to predict the stress-strain behavior of the plain-woven composite at the lamina level.

4.1 The four-cell model

To obtain analytical solution of mechanical property of composite material and keep the formulation simple, the cross section of the fill and warp yarns are assumed rectangular and their undulating form is approximated with only horizontal and inclined at angle θ sections as shown in Figure 4, where θ denotes the average undulation angle. In this approach investigated by Tanov and Tabiei (2001), RVC

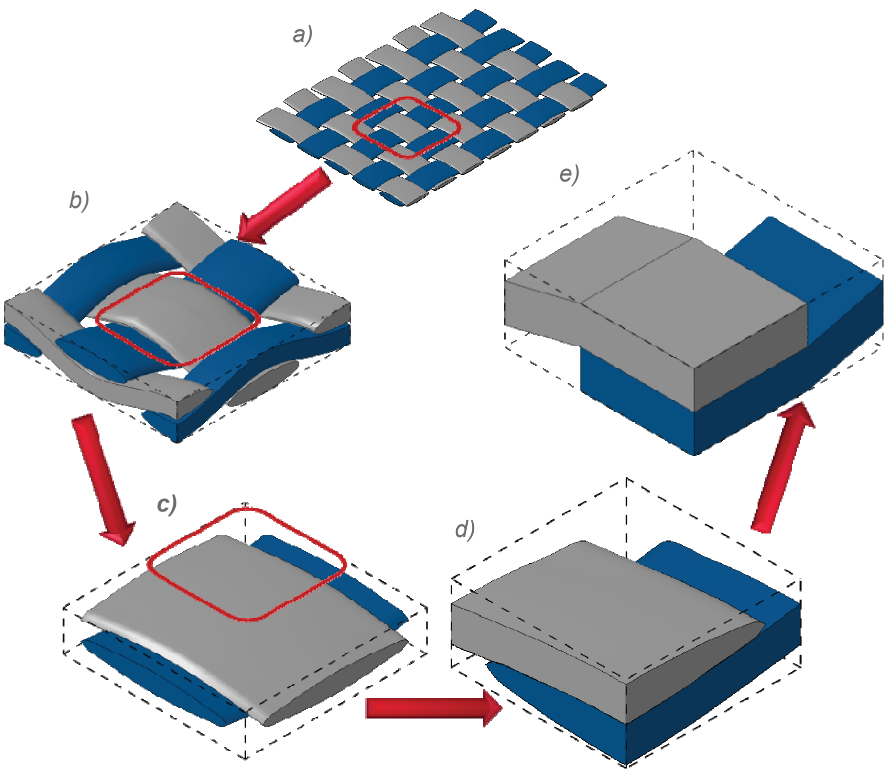

Figure 3: Woven fabric composite and micromechanical model: typical plain woven composites; representative volume cell andone quarter cell.

contains four sub-cells, i.e. sub-cell “ff”, “fm”, “mf” and “mm”. Sub-cell “fm” consists of yarn and matrix portions as illustrated in Figure 4.

From the geometry of the four-cell model, the height unit of RVC can be written as

$$H = 4(1 - V_y)\tan\theta \tag{30}$$

where V_y is overall yarn volume fraction, θ is the undulation angle. The width and depth of RVC is unit. Analytical solutions for the homogenization of the stiffness properties in Ref. by [Tanov and Tabiei (2001)] were derived based on the parallel-series assumptions such as for some of the strain components the adjacent cells are assumed to work in parallel and the corresponding strains are equal, while for the

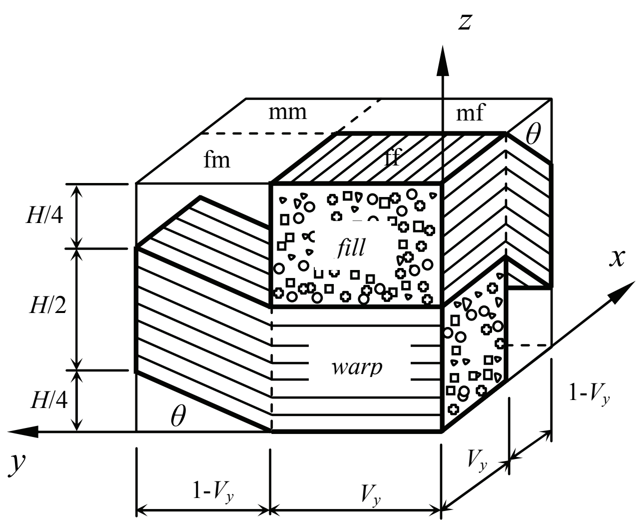

Figure 4: Geometry of the RVC for the four-cell model [Tanov and Tabiei(2001)].

rest of the strains, the cells are assumed to work in series, i.e. the corresponding stress components are equal and the strains are averaged to get the whole resultant strains. A similar parallel-series approach can be applied to the whole RVC and thus the sub-cell strains can be determined.

4.2 The smooth fabric models

Two 3D woven fabric composite unit cells were constructed to determine its elastic properties as shown in Figure 5(a) and (b). In this case, the fibers in yarn volume are unidirectional and smooth distributed along the fill/warp directions. We assume that the variation of bottom fiber in the fill direction on section $y = 0$ is

$$z_1(x) = z_0 - \frac{H}{4} + \frac{H}{4}\cos\frac{\pi x}{2} \tag{31a}$$

where z_0 denotes the location of a fibre at $x = y = 0$. For the bottom fibre, $z_0 = H/2$ and the fibre location in the *xoz* becomes

$$z_1(x) = \frac{H}{4}(1+\cos\frac{\pi x}{2}) \tag{31b}$$

Smooth fiber model I.

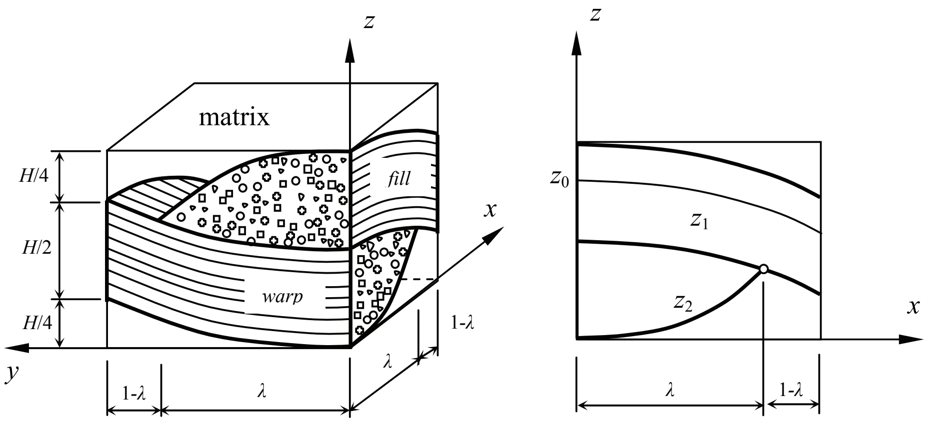

Figure 5: RVC with smooth fibres and geometry of yarn volume for model I.

The geometry of smooth fiber model I is illustrated in Figure 5. Suppose the configuration for the yarn volume in the warp direction to be

$$z_2(x) = \alpha x^2 \tag{32}$$

The coefficient α is determined by considering the location of joint for fibres of fill and warp

$$\alpha = \frac{H}{4\lambda^2}(1+\cos\frac{\pi\lambda}{2}) \tag{33}$$

where λ denotes the coordinate of joint shown in Figure 5. Considering the portion of fabric yarn volume in the RVC, we have following integral

$$V_y = 2\int_0^{\lambda} \left[\frac{H}{4}(1+\cos\frac{\pi x}{2}) - \alpha x^2\right] dx \tag{34}$$

Then we have following equation to evaluate the location of joint

$$4\lambda = 6V_y + 3(\lambda - \frac{2}{\pi}\sin\frac{\pi\lambda}{2}) - \lambda(1-\cos\frac{\pi\lambda}{2}) \tag{35}$$

The root of λ can be easily determined by the alterative method. Therefore, the top and bottom surfaces of yarn volume in warp direction can be written as

$$\begin{aligned}
z_{\text{bottom}}(x,y) &= \frac{H}{4}(1-\cos\frac{\pi y}{2})+\alpha x^2 \\
z_{\text{top}}(x,y) &= \frac{H}{2}+\frac{H}{4}(1-\cos\frac{\pi y}{2})-\left[\frac{H}{2}-\frac{H}{4}(1+\cos\frac{\pi x}{2})\right] \\
&= \frac{H}{4}(2+\cos\frac{\pi x}{2}-\cos\frac{\pi y}{2})
\end{aligned} \tag{36}$$

and the slop of fibres is

$$\frac{dz}{dy}=\frac{H\pi}{8}\sin\frac{\pi y}{2} \tag{37}$$

The derivative above will be used to determine the elasticity energy stored in yarn volume. Similarly to the yarn volume in fill direction, the top and bottom surfaces of yarn volume in warp direction can be written as

$$\begin{aligned}
z_{\text{top}}(x,y) &= H-\alpha y^2-\frac{H}{4}(1-\cos\frac{\pi x}{2}) \\
z_{\text{bottom}}(x,y) &= \frac{H}{4}(2+\cos\frac{\pi x}{2}-\cos\frac{\pi y}{2})
\end{aligned} \tag{38}$$

and the derivative of the fibre is

$$\frac{dz}{dx}=-\frac{H\pi}{8}\sin\frac{\pi x}{2} \tag{39}$$

Smooth fibre model II.

The geometry of smooth fiber model II is illustrated in Figure 6. The configuration for yarn volume in the warp direction is assumed to be a half of elliptic and defined as

$$z_2(x)=\frac{H}{4}(1\pm\sqrt{1-\frac{x^2}{\lambda^2}}) \tag{40}$$

where λ is the principle axis of elliptic which can be determined by the portion of yarn volume as

$$\lambda=\frac{4V_y}{\pi} \tag{41}$$

Model II is more suitable for a small portion of yarn volume composites. For instance, if the yarn volume portion $V_y = 0.5385$, then $\lambda = 0.8162$ and 0.6856 for the smooth fibre model I and model II respectively.

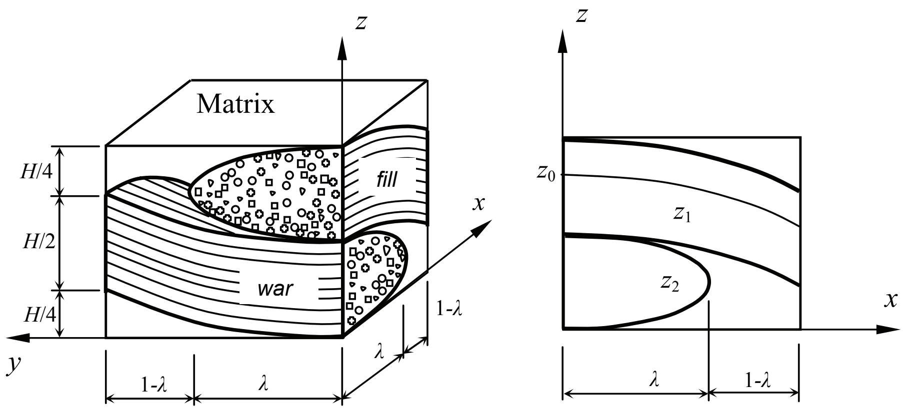

Figure 6: RVC with smooth fibres and geometry of yarn volume for model II.

5 Results and discussion

In this section, the application of mesh free method to the woven fabric composites is demonstrated. To deal with smooth fibre mode, we need to analyse transforming constitutive matrix by rotating the local coordinate system at angle θ respecting to the axis y. The fill constitutive matrix can be written as

$$\mathbf{C} = \begin{bmatrix} C_{11} & C_{12} & C_{12} & 0 & 0 & 0 \\ C_{12} & C_{22} & C_{23} & 0 & 0 & 0 \\ C_{12} & C_{23} & C_{22} & 0 & 0 & 0 \\ 0 & 0 & 0 & C_{44} & 0 & 0 \\ 0 & 0 & 0 & 0 & C_{55} & 0 \\ 0 & 0 & 0 & 0 & 0 & C_{44} \end{bmatrix}. \tag{42}$$

So the constitutive matrix in RVC global coordinate system by rotating the local system at angle θ becomes [Tanov and Tabiei(2001)]

$$\mathbf{C}'(\theta) = \begin{bmatrix} C'_{11} & C'_{12} & C'_{12} & 0 & 0 & C'_{16} \\ C'_{12} & C'_{22} & C'_{23} & 0 & 0 & C'_{26} \\ C'_{12} & C'_{23} & C'_{22} & 0 & 0 & C'_{36} \\ 0 & 0 & 0 & C'_{44} & C'_{45} & 0 \\ 0 & 0 & 0 & C'_{45} & C'_{55} & 0 \\ C'_{16} & C'_{26} & C'_{36} & 0 & 0 & C'_{66} \end{bmatrix} \tag{43}$$

where

$$
\begin{aligned}
C'_{11} &= C_{11}\cos^4\theta + C_{33}\sin^4\theta + 2(C_{13}+2C_{66})\sin^2\theta\cos^2\theta \\
C'_{12} &= C_{12}\cos^2\theta + C_{23}\sin^2\theta \\
C'_{13} &= C_{13}(\cos^4\theta + \sin^4\theta) + (C_{11}+C_{33}-4C_{66})\sin^2\theta\cos^2\theta \\
C'_{16} &= [(C_{13}-C_{11})\cos^2\theta + (C_{33}-C_{13})\sin^2\theta + 2C_{66}(\cos^2\theta-\sin^2\theta)]\sin^2\theta\cos^2\theta \\
C'_{22} &= C_{22}
\end{aligned}
\tag{44}
$$

$$
\begin{aligned}
C'_{23} &= C_{12}\sin^2\theta + C_{23}\cos^2\theta \\
C'_{26} &= (C_{23}-C_{12})\sin\theta\cos\theta \\
C'_{33} &= C_{11}\sin^4\theta + C_{33}\cos^4\theta + 2(C_{13}+2C_{66})\sin^2\theta\cos^2\theta \\
C'_{36} &= [(C_{13}-C_{11})\sin^2\theta + (C_{33}-C_{13})\cos^2\theta - 2C_{66}(\cos^2\theta-\sin^2\theta)]\sin^2\theta\cos^2\theta \\
C'_{44} &= C_{44}\cos^2\theta + C_{55}\sin^2\theta \\
C'_{45} &= (C_{55}-C_{44})\sin\theta\cos\theta \\
C'_{55} &= C_{44}\sin^4\theta + C_{55}\cos^4\theta \\
C'_{66} &= (C_{11}+C_{33}-2C_{13})\sin^2\theta\cos^2\theta + C_{66}(\cos^2\theta-\sin^2\theta)^2
\end{aligned}
$$

where θ is the angle of fibres and defined as from Eq. (39)

$$\theta = \tan^{-1}\left(\frac{H\pi}{8}\sin\frac{\pi x}{2}\right). \tag{45}$$

Similarly to the yarn in warp volume, the constitutive matrix is as follows

$$
\bar{\mathbf{C}}(\theta) = \begin{bmatrix}
C'_{11} & C'_{12} & C'_{12} & 0 & -C'_{16} & 0 \\
C'_{12} & C'_{22} & C'_{23} & 0 & -C'_{26} & 0 \\
C'_{12} & C'_{23} & C'_{22} & 0 & -C'_{36} & 0 \\
0 & 0 & 0 & C'_{44} & 0 & -C'_{45} \\
-C'_{16} & -C'_{26} & -C'_{36} & 0 & C'_{55} & 0 \\
0 & 0 & 0 & -C'_{45} & 0 & C'_{66}
\end{bmatrix}. \tag{46}
$$

where θ is the angle of fibres and defined as from Eq. (37)

$$\theta = \tan^{-1}\left(\frac{H\pi}{8}\sin\frac{\pi y}{2}\right). \tag{47}$$

A 3D woven fabric composite unit cell was constructed to determine its elastic properties by the finite element method by Chung and Tamma (1999). The RVC consists of epoxy matrix and fibre bundles, which are 65 percent E-glass/epoxy yarns and the properties are shown in Table 1. The yarn volume fraction $V_y = 0.5385$ and the average undulation angle attan $\theta = 1/6$. The thickness of the RVC is H=0.3077. The uniform distribution of nodes is shown in Figure 7. The total number of nodes is $N_x \times N_y \times N_z$ ($11\times11\times7$=847 in this paper) and the scale factors are selected by $\alpha_1 = \alpha_2 = 1;\ \alpha_3 = N_z/(N_x \times H)$. The elastic constants of RVC can be written as

$$\bar{\mathbf{C}} = \begin{bmatrix} \bar{C}_{11} & \bar{C}_{12} & \bar{C}_{13} & 0 & 0 & 0 \\ \bar{C}_{12} & \bar{C}_{11} & \bar{C}_{13} & 0 & 0 & 0 \\ \bar{C}_{12} & \bar{C}_{13} & \bar{C}_{33} & 0 & 0 & 0 \\ 0 & 0 & 0 & \bar{C}_{44} & 0 & 0 \\ 0 & 0 & 0 & 0 & \bar{C}_{55} & 0 \\ 0 & 0 & 0 & 0 & 0 & \bar{C}_{55} \end{bmatrix}. \tag{48}$$

Following calculations should be done to determine seven coefficients in above matrix:

Boundary conditions for

$\varepsilon_x = 1; \varepsilon_2 = \varepsilon_3 = \gamma_{xy} = \gamma_{yz} = \gamma_{zx} = 0$

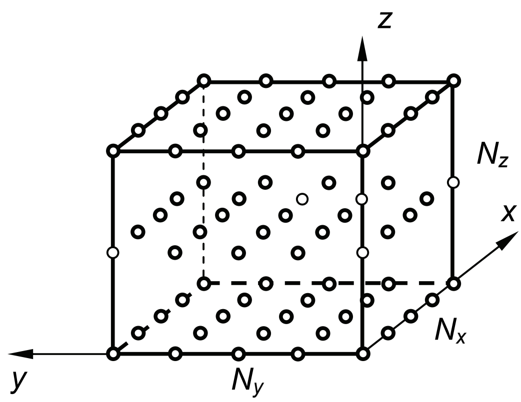

Figure 7: Uniform distribution of nodes in RVC ($5\times5\times3$).

Table 1: E-glass/epoxy properties

materials	E_x(GPa)	E_y(GPa)	G_{xy}(GPa)	G_{yz}(GPa)	ν_{xy}	ν_{yz}
Epoxy	3.5	3.5	1.3	1.3	0.35	0.35
Fiber bundles (65%)	47.77	18.02	5.494	3.877	0.314	0.249

$$x=0:\ u=0;\ \tau_{xy}=\tau_{zx}=0;\ \ x=1:\ u=1;\ \tau_{xy}=\tau_{zx}=0;$$
$$y=0: v=0;\ \tau_{xy}=\tau_{yz}=0;\ \ y=1:\ v=0;\ \tau_{xy}=\tau_{yz}=0; \tag{49}$$
$$z=0:\ w=0;\ \tau_{yz}=\tau_{zx}=0;\ \ z=H:\ w=0;\ \tau_{yz}=\tau_{zx}=0.$$

The total forces acting on three surfaces can be determined by following integral

$$F_x=\int_0^1\int_0^H \sigma_x|_{x=0}dzdy;\ F_y=\int_0^1\int_0^H \sigma_y|_{y=0}dzdx;\ F_z=\int_0^1\int_0^1 \sigma_z|_{z=0}dxdy. \tag{50}$$

Therefore, the micromechanical properties

$$\bar{C}_{11}=\frac{F_x}{H};\bar{C}_{12}=\frac{F_y}{H};\bar{C}_{13}=F_z. \tag{51}$$

Boundary conditions for

$$\varepsilon_z=1;\varepsilon_1=\varepsilon_1=\gamma_{xy}=\gamma_{yz}=\gamma_{zx}=0$$

$$x=0:\ u=0;\ \tau_{xy}=\tau_{zx}=0;\ \ x=1: u=0;\ \tau_{xy}=\tau_{zx}=0;$$
$$y=0: v=0;\ \tau_{xy}=\tau_{yz}=0;\ \ y=1:\ v=0;\ \tau_{xy}=\tau_{yz}=0; \tag{52}$$
$$z=0:\ w=0;\ \tau_{yz}=\tau_{zx}=0;\ \ z=H:\ w=H;\ \tau_{yz}=\tau_{zx}=0.$$

The total forces acting on three surfaces can be determined by following integral $F_z=\int_0^1\int_0^1 \sigma_z|_{z=0}dxdy$. Thus, the micromechanical property $\bar{C}_{33}=F_z$.
Boundary conditions for $\gamma_{xy}=1;\varepsilon_1=\varepsilon_2=\varepsilon_3=\gamma_{yz}=\gamma_{zx}=0$, can be achieved proximately by following displacements

$$x=0:\ v=0;\ \sigma_x=\tau_{zx}=0;\ \ x=1:\ v=1/2;\ \sigma_x=\tau_{zx}=0;$$
$$y=0:\ u=0;\ \sigma_y=\tau_{yz}=0;\ \ y=1:\ u=1/2;\ \sigma_y=\tau_{yz}=0; \tag{53}$$
$$z=0:\ w=0;\ \tau_{yz}=\tau_{zx}=0; z=H:\ w=0;\ \tau_{yz}=\tau_{zx}=0.$$

The total shear force can be written as $F_x=\int_0^1\int_0^H \tau_{xy}|_{y=0}dzdx$ and, therefore, the micromechanical property $\bar{C}_{44}=F_x/H$. Following the similar way, we can evaluate $\bar{C}_{55}$.
Table 2 shows the FEM results for the RVC properties from upper and lower bound estimates by Chung and Tamma (1999), Four/Single model results given by Tanov

and Tabiei (2001) and results by proposed method for different models. Compared with the numerical results given by FEM [Chung and Tamma (1999)], approximated analytical solution [Tanov and Taiebei(2001)] and the element-free Galerkin method, a good agreement has been achieved. Due to element mesh is free in this approach, the technique is more convenient and powerful dealing with complicated problems such as variation of fibre rotation in the VRC. For woven composites, we only need to define the smooth surfaces for both yarns in the fill and warp directions.

In the second example, a Glass/epoxy woven composite, which has been discussed by Marrey and Sankar (1977) by the FEM, with properties for the yarn $E_{\mathrm{L}} = 58.61\mathrm{GPa}$, $E_{\mathrm{T}} = 14.49\mathrm{GPa}$, $G_{\mathrm{LT}} = 5.38$, $\nu_{\mathrm{LT}} = 0.25$ and $\nu_{\mathrm{TT}} = 0.247$; the isotropic matrix is of Epoxy with $E = 3.45\mathrm{GPa}$, $\nu = 0.37$ is analyzed. The yarn volume fraction $V_y = 0.26$ and the average undulation angle $\theta = 4.2^0$. The thickness of RVC is H=0.2174. Table 3 shows all values obtained by using different approaches. It is shown that the agreement by the MLPG method is satisfied by comparing with other approaches.

In the last example, we consider a Graphite/epoxy RVC, which consists yarns with properties $E_{\mathrm{L}} = 137.3\mathrm{GPa}$, $E_{\mathrm{T}} = 10.79\mathrm{GPa}$, $G_{\mathrm{LT}} = 5.394$, $\nu_{\mathrm{LT}} = 0.26$ and $\nu_{\mathrm{TT}} = 0.46$; the isotropic matrix is of Epoxy with $E = 4.511\mathrm{GPa}$, $\nu = 0.38$. The yarn volume fraction, $V_y = 0.58$ and the average undulation angle at $\theta = 1.4^0$. From Eq. (30), the thickness of RVC is H=0.0411 unit. The numerical results by difference approaches are shown in Table 4. In general, good agreement is obtained with the approximated analytical solutions given by Tanov and Tabiei (2001) and element free Galerkin method. In the current approach, we consider the smooth woven fibers in the RVC only and believe that the prediction of micro mechanical properties using the meshless technique is more accurate.

6 Conclusions

The micromechanical models with smooth woven fabric composites have been established and studied numerically by using meshless local Petrov-Galerkin method. The distribution of the fibres in the RVC can be arbitrary in each numerical model and the prediction of micromechanical properties can be obtained easily by the proposed mesh free method. Compared with the results given by FEM and element-free Galerkin method, the accuracy of the MLPG method in this paper is satisfacroy. Similar to the element-free Galerkin method, we can conclude with following observations: (1) The smooth fibres model is more realistic; (2) The meshless local Petrov-Galerkin method is one of the most powerful method to evaluate moduli for micromechanical models; (3) More complicated woven fabric composite models can be investigated by the use of the MLPG method; (4) The MLPG method can be

Table 2: RVC properties by different approaches

Properties	Upper Bound Chung et al (1999)	Lower Bound Chung et al (1999)	Single-cell Model Tanov et al (2001)	Smooth Fibre Model I, Wen et al (2009)	Smooth Fibre Model II, Wen et al (2009)	Model I (MLPG)	Model II (MLPG)
C_{11} (GPa)	21.2	17.7	20.8	21.13	21.57	21.15	20.97
C_{12} (GPa)	5.4	5.4	5.29	5.28	5.25	5.35	5.27
C_{13} (GPa)	4.42	4.37	4.38	4.01	3.94	4.03	4.00
C_{33} (GPa)	9.82	9.23	9.23	8.75	8.41	8.95	8.82
C_{44} (GPa)	3.2	3.14	3.41	3.12	3.06	3.15	3.06
C_{55} (GPa)	2.42	2.23	2.29	2.35	2.25	2.28	2.33

Table 3: RVC properties by different approaches

Approach	E_x(GPa)	E_y(GPa)	G_{xz}, G_{yz}(GPa)	G_{xy}(GPa)	ν_{xy}	ν_{yz}
Ref [22]	11.81	6.14	1.84	2.15	0.408	0.181
Single-cell model Tanov et al (2001)	11.93	5.67	1.59	2.31	0.436	0.159
Smooth fibre model I Wen et al (2009)	12.81	5.80	1.625	1.94	0.438	0.149
Smooth fibre model II Wen et al (2009)	11.08	5.49	1.624	1.83	0.438	0.166
Model I (MLPG)	11.66	5.70	1.69	1.93	0.43	0.163
Model II (MLPG)	11.58	5.53	1.66	1.84	0.44	0.159

Table 4: RVC properties by different approaches

Approach	E_x(GPa)	E_y(GPa)	G_{xz}, G_{yz}(GPa)	G_{xy}(GPa)	ν_{xy}	ν_{yz}
Four-cell model Tanov et al (2001)	45.08	10.12	2.763	3.815	0.4643	0.0562
Single-cell model Tanov et al (2001)	45.17	9.782	2.585	3.813	0.4784	0.0542
Four-cell model Wen et al (2009)	45.21	9.930	2.873	3.337	0.4688	0.0559
Smooth fibre model I Wen et al (2009)	46.48	9.343	2.788	3.579	0.4913	0.0526
Smooth fibre model II Wen et al (2009)	46.29	9.176	2.834	3.506	o.4965	0.0526
Model I (MLPG)	44.86	9.338	2.530	3.546	0.4898	0.0538
Model II (MLPG)	44.84	9.228	2.509	3.459	0.4930	0.0545

extended to multi-scale progressive failure analysis.

References

Atluri, S.N.; Zhu, T. (1998a): A new meshless local Peyrov-Galerkin (MLPG) approach to nonlinear problems in computational modelling and simulation, *Comput Model Simul Engng,* vol. 3, pp. 187-196.

Atluri, S.N.; Zhu, T. (1998b): A new meshless local Peyrov-Galerkin (MLPG) approach in computational mechanics, *Comput. Mech.*, vol. 22, pp. 117-127.

Atluri, S.N.; Zhu, T., (1999): The meshlesss local Peyrov-Galerkin (MLPG) approach for solving problems in elasto-statics, *Comput. Mech.*, vol. 25, pp. 169-179.

Atluri, S.N. (2004): The Meshless Method (MLPG) for Domain and BIE Discretizations. Forsyth, GA, USA, Tech Science Press.

Atluri, S.N.; Liu, H.T.; Han, Z.D. (2005): Meshless Local Petrov-Galerkin (MLPG) Mixed Finite Difference Method for Solid Mechanics, *CMES: Computer Modeling in Engineering and Sciences*, vol. 15 (1), pp. 1-16.

Chung, P.W.; Tamma, K.K. (1999): Woven fabric composites – developments in engineering bounds, homogenization and application, *Int. J. Numer. Meth. Engng*, vol. 45, pp. 1757-1790.

Dang, Thi D.; Sankar, B.V. (2007): MLPG Formulation for Generalized Plane Strain Problems with Material Discontinuity and Application to Composite Micromechanics, *AIAA Journal* Vol. 45 (4), pp. 912-921.

Dang, Thi D.; Sankar, B.V. (2008): Meshless Local Petrov-Galerkin Micromechanical Analysis of Periodic Composites Including Shear Loadings, *CMES: Computer Modeling in Engineering & Sciences*, Vol. 6, No. 3, pp. 169-187.

Han, Z.D.; Liu, H.T.; Rajendran, A.M.; Atluri, S.N. (2006): The Applications of Meshless Local Petrov-Galerkin (MLPG) Approaches in High-Speed Impact, Penetration and Perforation Problems, *CMES: Computer Modeling in Engineering and Sciences*, vol. 14 (2), pp. 119-128.

Hardy, R.L. (1971): Multiquadric equations of topography and other irregular surface, J. Geophys. Res., vol. 76, pp. 1905-1915.

Ishikawa, T. (1981) Antisymmetric elastic properties of composite plates of satin weave cloth, Fibre Sci. Technol., vol. 15, pp. 127-145.

Ishikawa, T.; Chou, T.W. (1983): One-dimensional micromechanical analysis of woven fabric composites, *AIAA, J.,* vol.21 (12), pp. 1714-1721.

Jarak, T.; Soric, J.; Hoster, J. (2007): Analysis of shell deformation responses by the Meshless Local Petrov-Galerkin (MLPG) approach, *CMES: Computer Model-*

ing in Engineering and Sciences, vol. 18 (3), pp. 235-246.

Marrey,R.V.; Sankar, B.V. (1977): A micromechanical model for textile composite plate, *J. Compos. Mater.*, vol. 31 (12), pp. 1187-1213.

Sladek, J.; Sladek, V,; Wen, P.H.; Aliabadi, M.H. (2006): Meshless Local **Petrov-Galerkin** (MLPG) method for shear deformable shells analysis. *CMES: Computer Modeling in Engineering & Sciences*, vol. 13, pp. 103-117.

Sladek, J.; Sladek; V.; Zhang, Ch.; Solek, P. (2007a): Application of the MLPG to thermo-piezoelectricity, *CMES: Computer Modeling in Engineering and Sciences*, vol. 22 (3), pp. 217-233.

Sladek, J.; Sladek, V.; Zhang, Ch.; Solek, P.; Starek, L. (2007b): Fracture analyses in continuously nonhomogeneous piezoelectric solids by the MLPG, *CMES: Computer Modeling in Engineering and Sciences*, vol. 19 (3), pp. 247-262.

Sladek, J.; Sladek, V.; Zhang, Ch. (2004): Application of local integral equations to crack problems in FGMs, M.H. Aliabadi et al edited, Advances in Fracture and Damage Mechanics IV, EC Ltd, England, pp. 155-160.

Sladek, J.; Sladek, V.; Krivacek, J; Zhang, Ch. (2005a): Meshless local petrov-galerkin method for stress and crack analysis in 3-D axisymmetric FGM bodies, *CMES: Computer Modeling in Engineering and Sciences*, vol. 8(3), pp. 259-270.

Sladek, V.; Sladek, J.; Tanaka, M.; Zhang, Ch. (2005b): Local integral equation method for potential problems in functionally graded anisotropic materials, *Engng Analy. with Boundary Elements*, vol. 29, pp 829-843.

Tanov, R.; Tabiei, A. (2001): Computationally efficient micromechanical models for woven fabric composite elastic moduli, *J. App. Mech.*, vol. 68, pp. 553-560.

Wen, P.H.; Aliabadi, M.H. (2008): An Improved Meshless Collocation Method for Elastostatic and Elasto-dynamic Problems, *Journal Communications in Numerical Methods in Engineering*, vol. 24 (8), pp. 635-651.

Wen, P.H.; Aliabadi, M.H.; Liu, Y.W. (2008): Meshless method for crack analysis in functionally graded materials with enriched radial base functions *CMES: Computer Modeling in Engineering and Sciences*, vol. 30, pp. 133-147.

Wen, P.H.; Aliabadi, M.H. (2009a): Mesh-Free Micromechanical model for woven fabric composite elastic moduli, *Journal of Multiscale Modeling*, 1, 303-319.

Wen, P.H.; Aliabadi, M.H. (2009b): Evaluation of mixed-mode stress intensity factors by the mesh-free Galerkin method: static and dynamic. *Journal of Strain Analysis for Engineering Design*, vol. 44, pp. 273-86.

Wen, P.H.; Aliabadi, M.H. (2010): Mixed-mode stress intensity factors by mesh free Galerkin method. *Key Engineering Materials*, vol. 417-418, pp. 957-960.